DOI:
10.1117/1.JBO.21.3.036004

Document Version
Publisher's PDF, also known as Version of record

Journal of Biomedical Optics

BiomedicalOptics.SPIEDigitalLibrary.org

Optical coherence tomography use in the diagnosis of enamel defects

Khalifa Al-Azri
Lucia N. Melita
Adam P. Strange
Frederic Festy
Maisoon Al-Jawad
Richard Cook
Susan Parekh
Laurent Bozec

SPIE.

Khalifa Al-Azri, Lucia N. Melita, Adam P. Strange, Frederic Festy, Maisoon Al-Jawad, Richard Cook, Susan Parekh, Laurent Bozec, "Optical coherence tomography use in the diagnosis of enamel defects," *J. Biomed. Opt.* **21**(3), 036004 (), doi: 10.1117/1.JBO.21.3.036004.

Journal of Biomedical Optics 21(3), 036004 (March 2016)

Optical coherence tomography use in the diagnosis of enamel defects

Khalifa Al-Azri,[a] Lucia N. Melita,[b] Adam P. Strange,[b] Frederic Festy,[c] Maisoon Al-Jawad,[d] Richard Cook,[c] Susan Parekh,[a] and Laurent Bozec[b,*]

[a]University College London, Eastman Dental Institute, Paediatric Department, WC1X 8LD, London, United Kingdom
[b]University College London, Eastman Dental Institute, Biomaterials and Tissue Engineering, 308 Sussex Wing, WC1X 8LD, London, United Kingdom
[c]King's College London Dental Institute, Tissue Engineering and Biophotonics, Floor 17, Tower Wing, Guy's Hospital Campus, Great Maze Pond, London Bridge SE1 9RT, United Kingdom
[d]Queen Mary University of London, Barts and The London School of Medicine and Dentistry, London E1 4NS, United Kingdom

Abstract. Molar incisor hypomineralization (MIH) affects the permanent incisors and molars, whose undermineralized matrix is evidenced by lesions ranging from white to yellow/brown opacities to crumbling enamel lesions incapable of withstanding normal occlusal forces and function. Diagnosing the condition involves clinical and radiographic examination of these teeth, with known limitations in determining the depth extent of the enamel defects in particular. Optical coherence tomography (OCT) is an emerging hard and soft tissue imaging technique, which was investigated as a new potential diagnostic method in dentistry. A comparison between the diagnostic potential of the conventional methods and OCT was conducted. Compared to conventional imaging methods, OCT gave more information on the structure of the enamel defects as well as the depth extent of the defects into the enamel structure. Different types of enamel defects were compared, each type presenting a unique identifiable pattern when imaged using OCT. Additionally, advanced methods of OCT image analysis including backscattered light intensity profile analysis and enface reconstruction were performed. Both methods confirmed the potential of OCT in enamel defects diagnosis. In conclusion, OCT imaging enabled the identification of the type of enamel defect and the determination of the extent of the enamel defects in MIH with the advantage of being a radiation free diagnostic technique. [DOI: 10.1117/1.JBO.21.3.036004]

Keywords: optical coherence tomography; hypomineralization; diagnosis; enamel.

Paper 150694R received Oct. 15, 2015; accepted for publication Feb. 9, 2016; published online Mar. 10, 2016.

1 Introduction

Molar incisor hypomineralization (MIH) is defined as "hypomineralization of systemic origin affecting at least one first permanent molar (FPM), which is frequently associated with affected incisors."[1] The prevalence of MIH was reported to range from 2.8% to 25% in pediatric patients.[2] The significant variation in prevalence data can be related to the weakness of diagnostic criteria as MIH may often be confused with fluorosis or early carious (white spot) lesions. MIH can occur at any stage during the enamel formation and mineralization of FPMs and permanent incisors, which takes around 1000 days and continues for several years (~5 years). It has been suggested that the most critical period is the first year of life when early enamel maturation starts, particularly on first permanent incisors and FPMs.[3]

The etiology of MIH is still not completely understood and there is disagreement as to the criteria and factors that contribute to the correct diagnosis of this enamel defect.[4] Systematic reviews investigating the causative factors of MIH concluded that the best levels of evidence are either weak or moderate.[3,5] Enamel hypomineralization can occur in different clinical forms, ranging from mild to severe involvement. While less dramatic forms are characterized by porous and soft subsurface enamel, severe MIH can lead to posteruptive breakdown (PEB) of the affected enamel.[6] Once the FPMs come into occlusion, they start to break down as the enamel—even if bearing an intact surface—is substantially undermined within its depths and thus fundamentally weakened.[3] However, incisors do not generally show PEB, as they are not subjected to such substantial occlusal loads.[7,8]

Clinical features of MIH include opacities of large well-defined areas, ranging in color from white/creamy blemishes to yellow brown opacities. FPMs affected by MIH can be hypersensitive to hot and cold stimuli[2] and local anesthetic may not always be effective,[8] supposedly due to the porous enamel resulting in chronic clinically inflamed pulps.[9] Porous enamel may also facilitate the access of bacterial products causing inflammation of the pulp. Caries can progress rapidly in MIH teeth, making diagnosis difficult, especially if the tooth is badly broken down. It has been postulated that that children with very sensitive teeth might face difficulties during brushing, leading to poor oral hygiene and eventually caries.[8,10]

Currently, the main diagnostic method for MIH is clinical visual examination of the teeth. This can be performed with the aid of indices used to describe enamel defects, such as the modified developmental defects of enamel index (mDDE index)[11] or the European Association of Pediatric Dentistry (EAPD) MIH index, the latter requiring the examination of 12 permanent teeth (8 permanent incisors and 4 FPMs) at the age of eight.[4] Diagnosis at an early stage is key in the

*Address all correspondence to: Laurent Bozec, E-mail: l.bozec@ucl.ac.uk

management of MIH teeth, in order to reinforce oral hygiene, to maximize opportunities for teeth remineralization, and to reduce hypersensitivity. The available treatment options for MIH teeth are complex, ranging from prevention and restoration to extraction, depending on the patient's dental age, the severity of the condition, the child/parent's expectations, and background.[12] One major challenge is the assessment of the depth of the involved tissue, which has major impacts upon the specific design of the treatment plan to mask, remove, or cover the affected regions. Therefore, the determination of the extent of an MIH lesion into the enamel depths is crucial to determine the prognosis and treatment plan for affected teeth. However, this can be difficult to evaluate accurately solely from clinical examination, and as the lesions are superimposed on the bulk of the tooth structure. Similarly, such imaging modalities offer poor spatial resolution. Ultrahigh resolution clinical three-dimensional (3-D) techniques, such as cone beam computed tomography, necessitates significant radiological doses and are probably not justified in these scenarios, when no other radiological alternatives are possible.

The investigation of a more accurate diagnostic tool is important to enable us to determine the prognosis of affected teeth and, at the same time, gives an opportunity to move away from techniques, which expose patients to ionizing radiation. Optical coherence tomography (OCT) is a nondestructive imaging system, using a near-infrared (NIR) laser[13] to investigate the internal biological structures to a depth of up to 2 to 3 mm, depending on the light source and the scattering properties of the material of interest.[14,15] The image grayscale contrast obtained by OCT is the result of an interferometric correlation between the incident beam scattered by the sample and an equal length reference beam. In essence, OCT enables imaging the sample's structure at 2 to 3 mm depth, using partial time-coherence interferograms. This imaging depth is ideally suited to assessing full thickness of human enamel mantles, including the enamel-dentine junction (EDJ). The resulting image, also known as a B-scan, is two-dimensional (2-D) ($X - Z$) and is a direct measurement of the scattering and absorption properties of the underlying sample. Multiple B-scan images can be recorded in sequence in the Y-plane direction, resulting in the creation of a lateral tack of images that can be recomputed to form a 3-D image of the underlying sample—in this case, the enamel.

In dentistry, OCT has been used to investigate caries, artificial demineralization, and remineralization of enamel and dentine.[15–21] Jones et al.[15] used polarization-sensitive OCT (PS-OCT) to image artificial occlusal caries by investigating the magnitude of backscattered light with variations in the enamel volume.[15] They also used transverse sections from digital microradiography to obtain the quantitative mineral content profile and relative mineral loss. It was concluded that PS-OCT could be used to measure artificial occlusal caries by observing the changes in backscattering and depolarization of NIR light. The technique demonstrated its potential in detecting and monitoring early enamel caries.[15] A study conducted by Fried et al.[16] demonstrated that PS-OCT is an invaluable tool for imaging interproximal, occlusal, and early root caries and caries underneath composite fillings. Manesh et al.[19] also showed that PS-OCT can be used to detect remineralization of dentine. The aim of the present study was to prove that OCT could be used as a diagnostic tool in clinical practice for the noninvasive and noncontact cross-sectional investigation of enamel defects in a common enamel anomaly such as MIH.

2 Experimental Method

2.1 *Sample Collection*

Ethical approval for this study was obtained from the National Health Services Research Ethics Committee (NHS REC), United Kingdom (R & D reference number 11/LO/0777, Project ID: 11/0223), and 19 teeth were collected ($n = 19$) at the pediatric department at the Eastman Dental Hospital. Thirteen of them were MIH-affected FPMs ($n = 13$) and six were control teeth ($n = 6$). Following local hard tissue management protocols, the extracted teeth were collected and stored in 70% ethanol for 48 h at room temperature, before being debrided and stored in 0.1% aqueous thymol solution at 4°C (to maintain enamel hydration) until imaging.

2.2 *Photographic Imaging and Modified Developmental Defects of Enamel Index*

Photographs of the samples were taken using a Canon EOS Digital Rebel DS6041 equipped with a Canon Macro Ring Lite MR-14EX flash. Each sample was photographed against a dark background to enhance the contrast between the sample and the background (buccal, distal, lingual/palatal, and mesial surfaces were imaged). At this stage, the mDDE index was used to characterize the enamel lesions of the teeth, and each tooth surface was coded according to its location (L), demarcation (D), extent (E), and type of lesion (T).[11] Each code was graded according to severity of the lesion and was given grade 1 to 3, with 3 being most severe. This is summarized in Table 1.

2.3 *Radiographic Assessment*

Samples were imaged radiographically, immediately after the photographic investigation. Clinically relevant radiographic images for the control and the MIH-affected FPMs were performed on intraoral size 2 radiographic films—D speed

Table 1 Summary of the scoring indices and weighting used for the clinical diagnostics of MIH. Note that PEB refers to posteruptive breakdown.

	Location (L)	Demarcation (D)	Extent (E)	Type (T)
1	Occlusal half	Diffuse	<1/3 of surface involved	White creamy
2	Gingival half	Demarcated	1/3 to 2/3 of surface involved	Yellow brown
3	Whole surface	Both	<2/3 of surface involved	N/A
8	N/A	N/A	N/A	PEB

(Insight, Carestream Health, Inc., Rochester, New York, United States). For each tooth sample, two images were recorded: the first view was taken with the x-ray beam directed toward the buccolingual axis of the x-ray direction in order to image the mesial and distal surfaces, whereas the second view being taken with a perpendicular mesiodistal imaging axis was taken with the x-ray beam directed towards the mesiodistal direction in order to image the buccal and lingual surfaces.

2.4 *Histology and Polarization Microscopy*

A diamond-edged Accutom 5 rotary saw (Struers, Denmark) was used to cut the sample in cross-section near the MIH lesion of interest. Samples were cut into 2-mm-thick disks. Samples were then polished smooth by hand to ~300 μm thickness, using silicon carbide grinding paper grit 1200 (Struers, Denmark). The polished disks were washed in deionized water in an ultrasonic bath for 2 min.

For histological imaging, the disks were imaged using a Leica (Wetzlar, Germany) light microscope. This was equipped with a 5× magnification lens and two crossed light polarizers (90 deg) for optical polarization imaging. Images were captured using an 8-megapixel EOS Rebel t3i camera (Canon, Tokyo). Individual images were analyzed and stitched together to form a composite image using Photoshop processing software (Adobe, San Jose, California).

2.5 *Optical Coherence Tomography Scanning Instrument*

A VivoSight OCT scanner (Michelson Diagnostics, Kent, United Kingdom), based on a multibeam swept-source (SS) frequency domain was used during this research. It is equipped with a class I eye safe laser ($\lambda = 1305$ nm) and features an optical resolution in tissue of less than 7.5 μm laterally and less than 5 μm axially. The depth of focus of each of the four SSs is 1 mm and each is set 0.5 mm in advance of the previous one to enhance tissue penetration at higher resolution. The area scanned can be up to 6 mm × 6 mm (length × width), with an image depth of 1.2 to 2.0 mm depending on the tissue. The scan rate is 10 kHz and the frame rate can be up to 35 frames per second. The images are presented as stacks of vertical B-scans for a total of 600 frames, acquired at a distance of 10 μm between each frame. As such, each frames measured 6 mm width and about 1.84 mm depth (in the XZ or B scan dimensions). The images were then exported from OCT software as 16-bit TIFF images.

Each tooth sample was taken from the storage medium and the excess moisture removed before being mounted on the instrument imaging stage. For reproducibility and image stability, the handheld OCT probe was mounted onto a movable arm. All scans started at or close to the cemento-enamel junction (CEJ) cervically and ended at the cusps occlusally. Each of the tooth surfaces (buccal, distal, lingual/palatal, and mesial) were imaged regardless of the presence of MIH lesion. Occlusal surfaces were not scanned due to their complex morphology and the presence of restorations in some of the samples.

2.6 *Image Processing*

All OCT images, either as single frames or as a full stack of images, were processed using Image J software (Image J 1.47 with 64-bit Java, 2013, Bethesda, Maryland, United States). For conciseness of the report, the single frames presented were randomly selected from a stack of interest (either control or MIH) and found to be representative of the overall scattering pattern observed within the image stacks. Additionally, the scattering profiles were extracted from each frame and plotted as a function of sample's depth, using Origin Pro 9.0 (Origin Lab Corporation, Northampton, Massachusetts, United States). The regions selected to obtain the scattering profiles from the randomly selected single frame were also chosen at random to ensure that the analysis avoided sampling bias. All distances presented on the *X*-axis of the scattering profiles plotted are defined as optical rather than absolute distances as they have not been corrected for the indices of refraction.

3 Results and Discussion

3.1 *Clinical Photographs*

The photographic images of MIH teeth were examined and the mDDE index was used to characterize the MIH lesions. An example of the phenotypic characterization in Fig. 1 shows the buccal surface of an upper-right FPM with an MIH lesion. The whole of the tooth surface is involved, consequently code L3 is assigned. Additionally, the lesion is both demarcated and diffuse resulting in a code of D3 for demarcation. At least two-thirds of the tooth is affected; therefore, E3 is given for the extent of the lesion. Three types of MIH enamel defects are detected: type 1, white creamy lesion (T1); type 2, yellow-brown lesion (T2); and type 8, PEB (T8). Table 2 summarizes the mDDE index score for the enamel defects present in all MIH-affected FPMs.

This index is used routinely in clinics and forms part of the clinical assessment. However, this index describes only the external features of each lesion and does not give any indication of the impact of the lesion on the internal structure of each tooth surface. For example, there are no means to evaluate whether the MIH lesion is affecting the entire enamel thickness or whether the lesion is affected subsurface by cracks, which may lead to PEB. However, a study by Farah et al.[22] showed that such visual

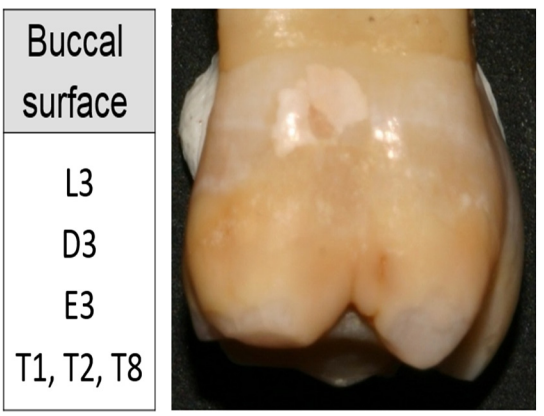

Fig. 1 Example of the phenotypic characterization of the buccal surface of an upper-right FPM with a MIH lesion. The whole of the tooth surface is involved, consequently code L3 is assigned. Additionally, the lesion is both demarcated and diffuse, resulting in a code of D3 for demarcation. At least two-thirds of the tooth is affected; therefore, E3 is given for the extent of the lesion.

Table 2 Summary of the mDDE index scores of the enamel defects present in all MIH-affected FPM teeth used as part of this study.

Tooth sample	Location (L)	Demarcation (D)	Extent of defect (E)	Type of defect (T)
MIH 1	L3	D3	E3	T2
MIH 2	L3	D3	E3	T1 and T8
MIH 3	L3	D3	E3	T2 and T8
MIH 4	L3	D3	E3	T1
MIH 5	L3	D2	E3	T1 and T8
MIH 6	L1	D1	E1	T2 and T8
MIH 7	L3	D3	E3	T1 and T8
MIH 8	L3	D3	E3	T1 and T8
MIH 9	L3	D3	E3	T1 and T8
MIH 10	L3	D3	E3	T1 and T8
MIH 11	L3	D2	E3	T1
MIH 12	L3	D3	E3	T2
MIH 13	L1	D2	E2	T1 and T8

assessment of the degree of staining of MIH-affected teeth may be used to clinically reflect the severity of the defect but should be used in combination with other diagnostics approaches. An alternative index, the molar hypomineralization severity index (MHSI), was investigated by Oliver et al.[23] in 2014, to determine treatment of defects in MIH based on their clinical characteristics. Their study showed that treatment modalities are dependent on color and location of defects, and the amount of PEB affecting FPMs.

This index was not available when the current study was started in 2012, but the mDDE index used to cover the same characteristics of location, color, and PEB. While the MHSI is useful for clinical management, it does not aid in diagnosis of defects, as many children present in the early mixed dentition before all the FPMs and permanent incisors have erupted. Therefore, the mDDE index, which can be used to record all enamel defects, irrespective of clinical diagnosis, is more useful.

3.2 *Radiographic Examination*

Radiographic imaging is one of the most common diagnostic tools used in the field of dentistry. Although efforts are made to reduce the ionizing radiation exposure to patients and practitioners, by principles of justification and optimization of radiographic imaging, the versatile use of x-ray imaging is still a cause for concern for individual safety. From a diagnostics point of view, radiographic imaging produces 2-D images of 3-D teeth. In the context of MIH diagnostics, it is used to demonstrate the extent of the lesion and determine mainly if the lesion is severe. Figure 2 shows a comparison between clinical photographs and radiographs for both control tooth [Figs. 2(a) and 2(b)] and MIH-affected tooth [Figs. 2(c) and 2(d)].

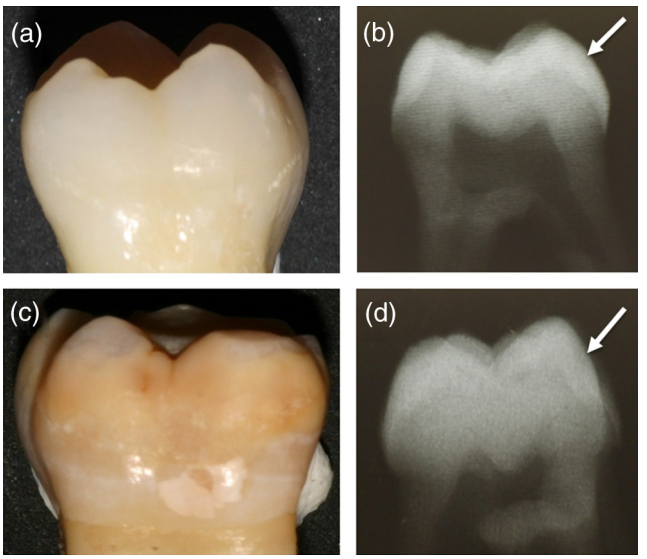

Fig. 2 Clinical photographs and radiographic images of (a and b) a control tooth and (c and d) an MIH-affected tooth. The mesiodistal view of the tooth is presented in the clinical photograph (a–c), whereas it is the buccolingual view that is presented in the radiographic image (b–d) in an effort to observe the depth of penetration of the MIH lesion. The arrows point to the same area for both teeth, highlighting the area affected with MIH (d) and its corresponding healthy control area (b).

On the radiographic images of both control and MIH-affected teeth, the different surfaces are superimposed, making it difficult to discern specific features, besides the EDJ, the CEJ, and pulp chamber. However, the occlusal, mesial, and distal surfaces can be examined in detail without shading as a result of the 3-D projection. From a diagnostic point of view, these images are of low resolution and even though the whole dental crown (enamel, EDJ, dentine, and the dental pulp) can be seen clearly, radiographic images cannot show fine details of these structures, such as disorganized enamel, change in mineralization, or cracks within the enamel formation. This lack of ability to resolve finer enamel structures or defects may enhance diagnostic errors, particularly with regards to lesion depth extent, although they can be visually identified at the surface of the enamel. This effectively reduces the pertinence of the diagnostics.

3.3 *Optical Coherence Tomography Imaging of Healthy and Molar Incisor Hypomineralization Affected Tooth*

3.3.1 *Control teeth*

An example of a single-frame OCT image of a healthy enamel layer from a control tooth is shown in Fig. 3(b). In this example, a palatal surface of an upper-right FPM was imaged, as shown in the clinical photograph in Fig. 3(a). The dotted square area drawn on the tooth surface is representative of the 6 mm × 6 mm scanning window preset by the instrument. Figure 3(b) is a representative single-frame OCT image (B-scan) of healthy enamel. The enamel and dentine layers are labeled 1 and 2, respectively, and the EDJ is labeled as 3 in Fig. 3(b). The interface between the air (dark area above the enamel) and the enamel appears particularly bright due to the high scattering of the incident photons as they encounter a

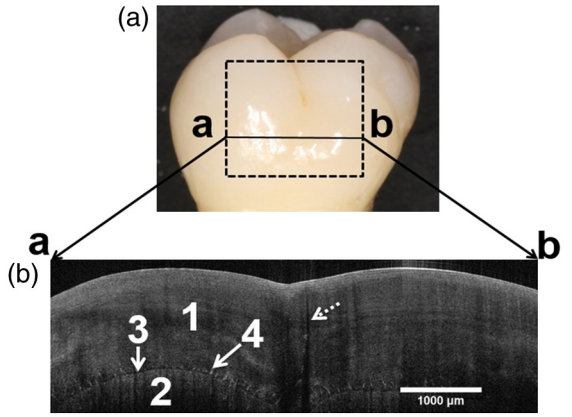

Fig. 3 (a) Clinical photograph of a palatal surface of an upper-right control FPM and a representative single-frame OCT image (B-scan) taken from the OCT stacks recorded with the dotted square area drawn on the tooth surface. (b) The enamel and dentine layers are labeled 1 and 2, respectively, and the EDJ is labeled as 3. Needle-like structures associated with the EDJ, labeled 4, may correspond to enamel spindles. An enamel crack can also be observed (dotted arrow).

region with a high refractive index and with an uneven surface topography.

The transmitted photons penetrate the enamel layer and were reflected by the internal enamel features. Although intensity was reduced from greater depths by increased scattering, any structural changes in the enamel layer induced a new scattering front, which was demonstrated as a brighter line or region in the grayscale image. Subtle variations in the grayscale contrast of the image could also be indicative of small variations in the enamel mineral contents. It is also possible to distinguish small needle-like structures associated with the EDJ [labeled 4 on Fig. 3(b)], which possibly correspond to either enamel spindles as seen histologically, or alternatively, small cracks across the EDJ.

Another type of feature frequently seen in OCT images is enamel crack lines, which may run from the enamel surface toward the EDJ or from the EDJ toward the enamel surface as demonstrated by the dotted arrow [Fig. 3(b)]. OCT is particularly efficient at detecting these fine crack lines, as their presence is usually amplified by an increase of scattering light, as demonstrated by Imai et al.[24] and a resulting shadowing effect presented as a darker region immediately below the crack on the B-scan. The shadowing effect can be considered as an imaging artifact, but in practice, it allows the rapid detection of crack lines that are sometimes barely visible.

3.3.2 *Correlation between histology and optical coherence tomography imaging on a molar incisor hypomineralization affected tooth*

Previous studies have tried to correlate *in vivo* OCT with *ex vivo* histology.[25] Although the current study only investigates *ex vivo* teeth, a similar approach was used. Figure 4(a) shows the clinical photograph of an MIH tooth with a diffuse T2 MIH lesion as an example for the correlation between these techniques. OCT imaging [Fig. 4(d)] was performed on the tooth along the marked line, as shown in Fig. 4(a), prior to any further histology preparation. Histology sectioning was then performed on the tooth before polishing the section down to a thickness of 250 μm to allow for histology imaging. During the cutting procedure, a portion of the T2 lesions broke off, as highlighted by the arrow in Fig. 4(b). This occurred frequently, as the MIH-affected area of the tooth is mechanically weaker when compared to its surrounding healthy enamel. It is also likely that there may have been underlying undetected PEB present at that location. Nonetheless, the separate regions, healthy and MIH affected, are evident in Fig. 4(b). The presence of the MIH lesion near the occlusal surface becomes more apparent while imaging the section under polarization microscopy. Under this mode of imaging, the healthy enamel appears opalescent, whereas the MIH-affected enamel is more opaque. Although this T2 lesion near the occlusal part of the tooth was damaged during the histological process, it is still possible to correlate the OCT scan with the histology sectioning. The star shows the location of the healthy enamel on both imaging mode (polarization microscopy and OCT) lesion, whereas the triangle shows the MIH-affected area. The correlation between the two areas matches accurately and the interface between healthy and affected enamel becomes clearer in the case of OCT imaging. In 2008, Hirasuna et al.[26] used PS-OCT and NIR to monitor early carious lesions. In their approach, they also used a digital microradiography system to quantify the enamel defect severity by measurement of the relative mineral loss for comparison with optical scattering measurements. Developmental defects were clearly visible in the polarization-resolved OCT images, demonstrating that PS-OCT could be utilized to nondestructively

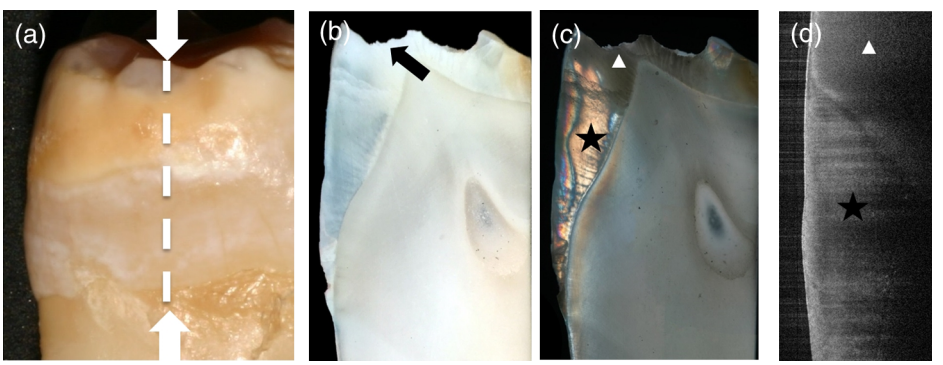

Fig. 4 (a) Clinical photograph of a buccal surface of an MIH diffuse T2 (top) defects, the dotted lines show the OCT scan area. (b) Histology image of tooth at 5× magnification with the arrow indicating loss of enamel due to PEB. (c) Polarized histology image of tooth, with T1 defect starred at 5× magnification (d) OCT image of the MIH diffuse T2 area.

measure the depth and possible severity of the defects. With the recent improvements made in OCT resolution and speed, combined with the vulnerability of the MIH teeth to damage, the nondestructive *in vivo* OCT technique should be preferred over the *ex vivo* destructive histological analysis.

3.4 *Qualitative Diagnostics of Molar Incisor Hypomineralization Types Using Optical Coherence Tomography Imaging*

3.4.1 *Type 1 (white/creamy) molar incisor hypomineralization defect*

Figure 5(b) shows the image of diffuse type 1 defect, a white creamy MIH defect present on the palatal surface of the affected tooth. According to the mDDE index in Fig. 5(a), the defect is located on the whole surface of the tooth (L3), diffuse (D2), and extending at least two-thirds of the surface (E3). Three representative OCT scans were chosen in Fig. 5(c) to demonstrate the appearance of this type of MIH defect (diffuse type 1 defect). The dotted lines highlight where the OCT scans were taken. The defect is mainly affecting the distal half of the tooth surface while part of the mesial half is spared especially in Figs. 5(c1) and 5(c2). In Fig. 5(c3), the enamel is broken in the mesial side, as observed in the clinical picture in Fig. 5(b).

It can be seen that there is an increase in the scattering of the photons just below the enamel surface, as shown by the solid white arrow. Because of the high level of scattering present in that region, there is a significant amount of shadowing occurring, meaning that it proves difficult to evaluate the intactness of the enamel layer below that critical region. However, the OCT image clearly demonstrates that the region adjacent to that critically scattering region is healthy.

An example of demarcated type 1 defect is found in the buccal surface of the affected tooth shown in Fig. 6(b). The tooth presents two types of defects: the demarcated type 1 white creamy defect and the diffuse (D2) type 2 yellow brown defect, which is shown in Fig. 7. According to the mDDE index MIH, it involves the whole surface of the tooth (L3) and extends to more than two-thirds of the surface (E3) in Fig. 6(a). However, the description of this defect using mDDE index does not give us enough information on the extent of the lesion deep into enamel. It superficially describes the defect extent across the surface.

The OCT scans are located at the occlusal and cervical ends of the defect, respectively. In a similar manner to Fig. 5(c), the OCT images of demarcated type 1 defect in Fig. 6(c) show an irregular crack line about 2 mm long below the surface of the enamel. On the right-hand side of the scans, it is possible to see that the crack line has erupted at the enamel surface. From a diagnostic point of view, it is likely that this tooth may lose over time the entire enamel section sitting above the crack line, effectively creating a PEB.

3.4.2 *Type 2 (yellow/brown) molar incisor hypomineralization defect*

Figures 7 and 8 show OCT images obtained, respectively, from diffuse and demarcated type 2 defects. In Fig. 7(a), according to the mDDE index, the yellow brown defect involves the buccal half of the surface (L3), diffuse (D3), and it extended across the whole surface of the tooth (E3). The OCT scan in Fig. 7(c) shows the appearance of the diffuse type 2 defect present on the surface. The white arrows in Figs. 7(b1), 7(b2), and 7(b3) indicate the defect extension into enamel. The image contrast at the surface appears gradually brighter than the surrounding enamel, especially near the enamel surface. The area below this bright band of subsurface enamel has significant shadowing, rendering the enamel below dark, with difficulties in assessing the quality of the enamel structure.

In the case of the demarcated type 2 (Fig. 8), the defect is localized in the occlusal half of the surface (L1), demarcated (D1), and extends to about a third of the surface (E1). The palatal defect (white arrow) is visible in all the corresponding OCT sequence [Fig. 8(c)], initiating close to the EDJ [Fig. 8(c5)] and progressing to the surface of the enamel [Fig. 8(c1)]. As it spreads across the palatal side of the distal surface, it exhibits featureless appearance with loss of normal scattering of light,

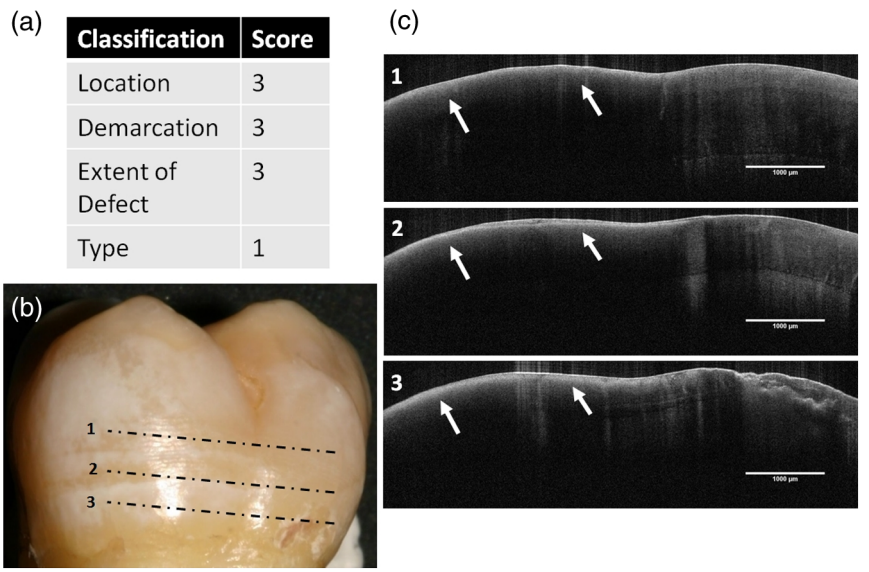

Fig. 5 (a) MIH-affected tooth showing a diffuse T1 defect. (b) Clinical photograph of a palatal surface with the locations labeled as 1, 2, 3 corresponding to the (c) OCT cross-sectional images.

(a)

Classification	Score
Location	3
Demarcation	3
Extent of Defect	3
Type	1/8

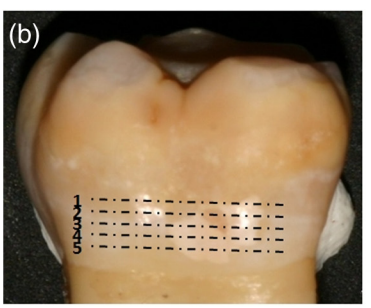

(c)

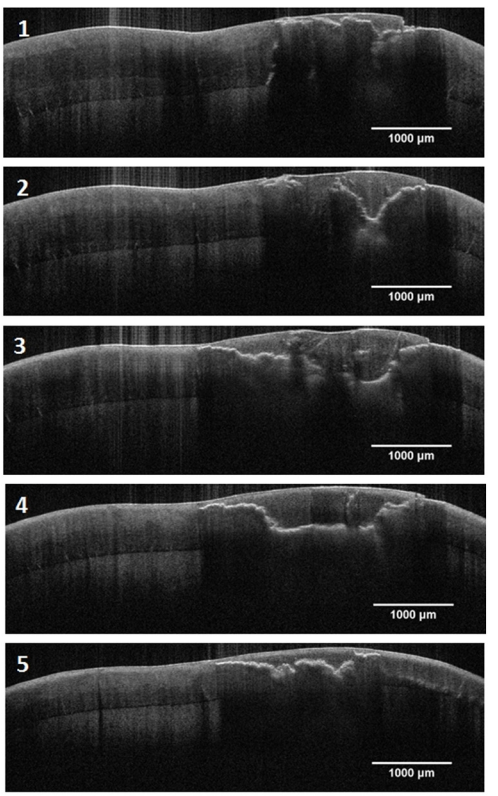

Fig. 6 (a) MIH-affected tooth showing a demarcated T1 defect. (b) Clinical photograph of a buccal surface with the locations labeled as 1, 2, 3, 4, and 5 corresponding to the (c) OCT cross-sectional images.

(a)

Classification	Score
Location	3
Demarcation	3
Extent of Defect	3
Type	2

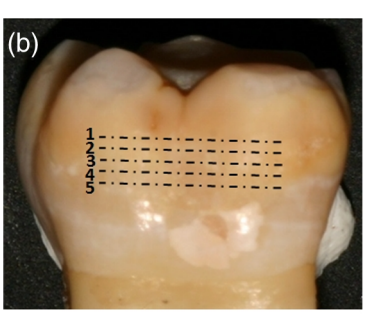

(c)

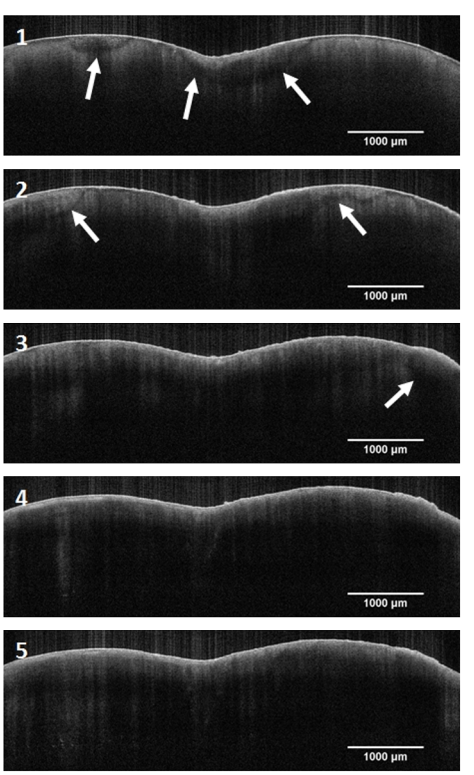

Fig. 7 (a) MIH-affected tooth showing a diffuse T2 defect. (b) Clinical photograph of a buccal surface with the locations labeled 1, 2, 3, 4, and 5 corresponding to the (c) OCT cross-sectional images.

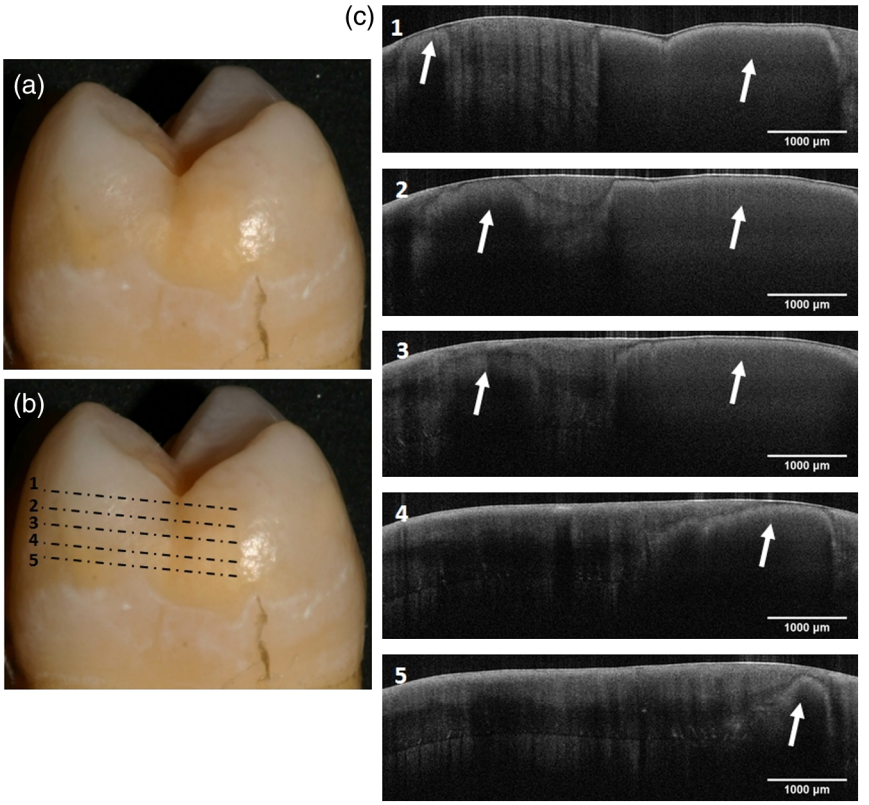

Fig. 8 (a) MIH-affected tooth showing a demarcated T2 defect. (b) Clinical photograph of a distal surface (b) with the locations labeled 1, 2, 3, 4, and 5 corresponding to the (c) OCT cross-sectional images.

normally expected in healthy enamel. The image contrast is very homogeneous with a featureless appearance of enamel in the deeper region below the surface. It is worth noting the narrow bright band just below the enamel surface.

3.4.3 *Type 8 (with posteruptive breakdown) molar incisor hypomineralization defect*

Figure 9 shows a tooth affected by a type 8 defect on the occlusal surface. The defect is confined occlusally to the buccal cusps with a yellow brown halo around it. According to the mDDE index in Fig. 9(a), the defect is localized in the occlusal half of the tooth (L1), demarcated (D1), and its extent is less than a third of the tooth (E1). Previously, Fig. 6(c1) indicated the position of the OCT frames selected close to the PEB region occlusally. The OCT images [Fig. 9(c)] show the appearance of the defect in enamel, as indicated by the arrow. The images were taken from the buccal surface close to the PEB. The white arrows indicate a fracture line extending into the enamel surface, which could have propagated from the area close to the PEB [Fig. 9(c1)] down to into the cervical area [Fig. 9(c5)], suggesting that the surface is weakened by the breakdown, which occurred occlusally.

A second example is shown in Fig. 10. The occlusal surface is affected by a type 2 defect in Fig. 10(b), but it is closely situated to a type 8 PEB from Fig. 9(b). According to the mDDE index in Fig. 10(a), the MIH defect is located on the occlusal half (L1), demarcated (D1), and it extends to less than a third of the surface (E1). The corresponding OCT images [Fig. (10c)] show the extent of the defect deep into enamel. Although the region from which these images were taken was classified clinically as unaffected, the enamel seemed severely affected on the OCT. The breakdown in enamel appears to begin from the EDJ, indicated by the white arrows and becomes more evident dividing the thickness of enamel into two layers, leading to PEB. The blue arrows in the OCT scans highlight the presence of a crack extending from the enamel surface to the EDJ. The diagnosis of this feature is important as it helps clinicians to determine the prognosis of the tooth as it weakens.

3.4.4 *Merits of qualitative diagnostics using optical coherence tomography imaging*

One key outcome of this qualitative diagnostics study using OCT imaging is to appreciate the complexity of the scattering images recorded by OCT. To make the most of these images, clinicians need some knowledge regarding how the instrument produces these images in order to refine their understanding of the variation in image contrast. The use of OCT as a diagnostic method has some advantages when characterizing MIH-affected teeth compared to clinical and radiographic methods. It is possible to visualize the subsurface structure of enamel with a high spatial resolution (5 μm) and the details obtained from these images can only be obtained microscopically. This is consistent with the result obtained by a previous study.[27] By using OCT for the diagnosis of MIH lesions, one key element is to be able to assess the depth of each of these lesions once they have been clearly identified, allowing the clinician to plan their approaches to masking the lesions by informing the depth of the defects and whether external adhesive or coronal encircling restorations are more appropriate.

(a)

Classification	Score
Location	1
Demarcation	1
Extent of Defect	1
Type	8

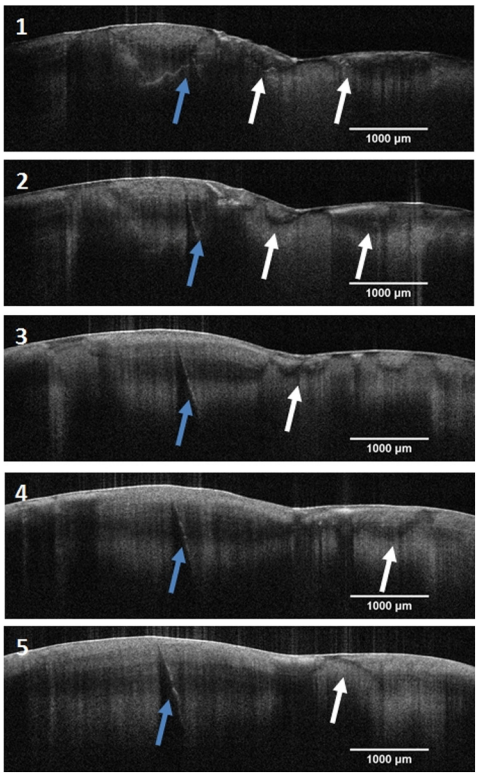

Fig. 9 (a) MIH-affected tooth showing a T8 defect with PEB. (b) Clinical photograph of a buccal surface with the locations labeled 1, 2, 3, 4 and 5 corresponding to the (c) OCT cross-sectional images.

(a)

Classification	Score
Location	1
Demarcation	1
Extent of Defect	1
Type	2

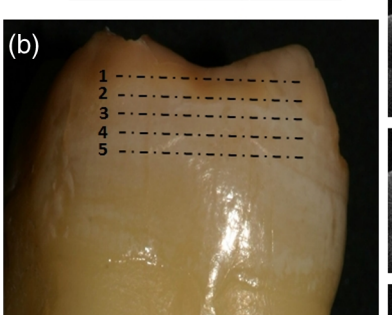

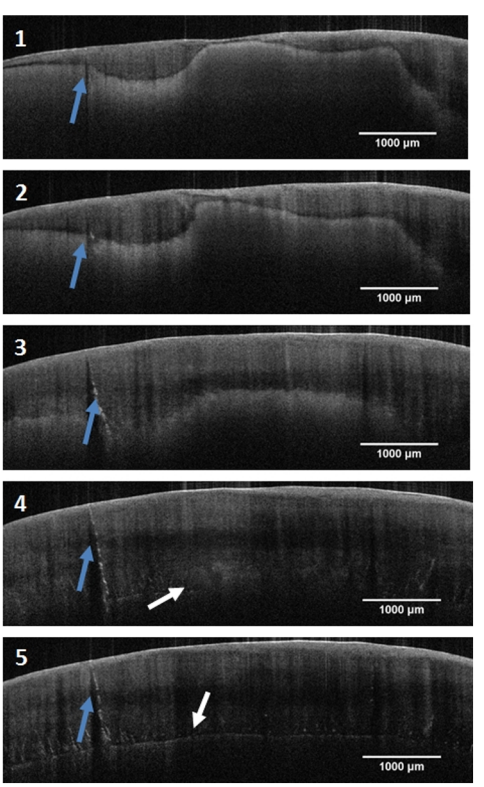

Fig. 10 (a) MIH-affected tooth showing a T2 defect. (b) Clinical photograph of an occlusal surface with the locations labeled as 1, 2, 3, 4, and 5 corresponding to the (c) OCT cross-sectional images.

The plurality of scattering behaviors represented in the different types of MIH enamel defect is also indicative that MIH as a condition is poorly understood in terms of enamel structure versus MIH type and that more research is required to understand these correlations. One of the most encouraging early publications, presenting OCT as possible clinical diagnostics tool, was performed by Louie et al.[25] They tested the hypothesis that PS-OCT may be used to nondestructively measure and quantify the severity of the early demineralization of enamel on buccal and occlusal surfaces and assess the inhibitory effect of fluoride varnish *in vivo*. In their study, high-contrast PS-OCT images were acquired of both occlusal and buccal surfaces *in vivo*. Both occlusal and buccal surfaces showed a significant difference ($P < 0.05$) in the integrated reflectivity (ΔR) between the "sound" and "carious" enamel groups.

Like the work present by Louie et al.,[25] our analysis from a nonpolarizing OCT system presented single frames for each of the key MIH lesion, but in fact, each of the scans collected 600 frames. This is a significant amount of data for any clinical team to process and use in their diagnostics. The current method of qualitative diagnostics is informative, but more work is required to establish specific databases where clinicians could compare their scan with defined cases. The main disadvantage of this approach is that the maximum depth of imaging is about 2 mm and ~1.8 mm of enamel could be successfully imaged. Though it is a sufficient depth for scanning enamel in some regions, the EDJ may be beyond resolution in the region of the cusps of the teeth, where the thickness is often above 2 mm. More complex enamel structures here would need more interpretation—smooth surfaces affording clearer understanding of enamel derangements and allow chronological interpretation of the likely occlusal and cuspal depths of involvement.

4 Advanced Diagnostics Using Optical Coherence Tomography

4.1 *Scattering Profiles*

In order to assess the merit of using OCT for a more systematic diagnostic dental application, OCT images were further analyzed. To do so, scattering profiles as a function of the enamel depth were measured in selected B-scans of both control and MIH teeth. These profiles provide a direct representation of the scattering of photons as they travel through the enamel layer and any disruption in the enamel structure may result in scattering that can be measured in the profile. Figure 11 shows the results of such an approach on a control sample. For consistency, each scattering profile is the average of a 10-pixel (40.5 μm) width area in the X-axis.

The subsequent profiles were then plotted as function of depth before being normalized to the enamel/air scattering peak. Figure 11(b) shows a series of profiles that have been obtained within the same B-scan, as shown in Fig. 11(a). These profiles were usually characterized by an initial nonscattering phase when the photons are travelling through the air before they encounter the enamel surface. At this stage, the profile exhibits a very strong scattering peak as the photons encounter a medium with a greater refraction index ($n \sim 1.63$)[28,29] compared to air ($n = 1$). Following this strong scattering peak, the profile presents a decay profile as the photons become progressively more scattered as their bidirectional journey includes greater depths of the scattering sample of enamel, as shown in Fig. 11(c). It is worth noting that the decay of the scattering profiles in healthy enamel may present some small variations, which are due to localized interruptions in the enamel structural and chemical homogeneity. These could relate to normal variations of structure, including enamel spindles or small

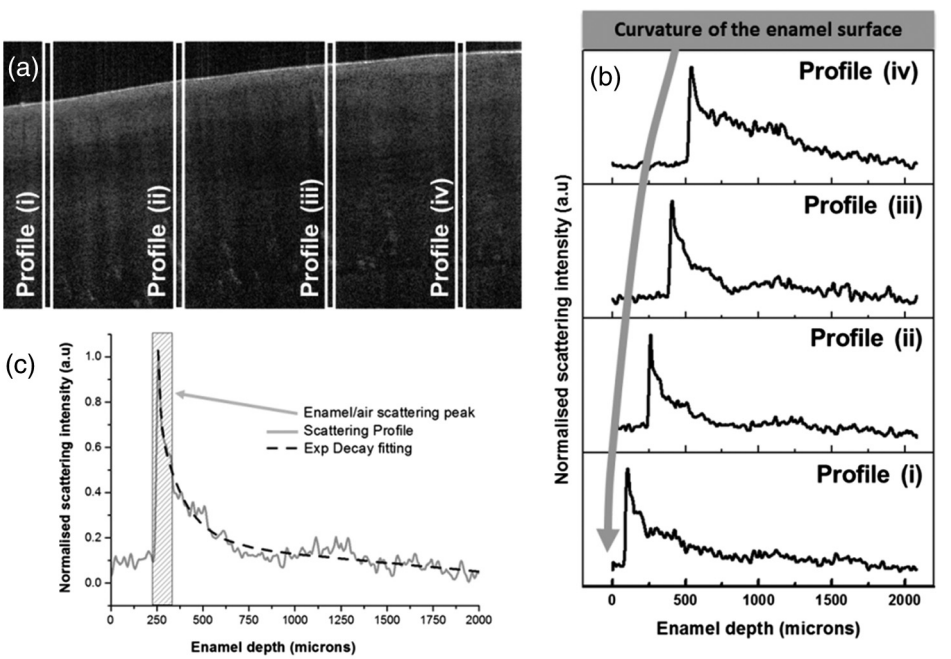

Fig. 11 (a) OCT image of healthy enamel used for scattering profiles analysis selected randomly from a full stack (600 images). (b) The scattering profiles (average of 10 individual pixel columns) plotted at a function of enamel depth from random location in (a). The large arrow in (b) indicates the surface curvature of the enamel. (c) The scattering profile observed for healthy enamel is summarized.

cracks in the proximity of the EDJ. It is also necessary to consider that the nonscattering phase prior to the enamel/air scattering peak will vary from profile to profile because of the curvature of the enamel surface while recording the profiles.

The same approach was performed on B-scans obtained from an MIH-affected tooth. Again, several profiles were recorded at different locations within B-scan as shown, respectively, in Fig. 12(a). A similar enamel–air scattering peak was recorded as the control healthy enamel. However, the overall shape of the profiles dramatically changed while penetrating deeper in the enamel layer. In all profiles presented in Fig. 12(b), it is possible to observe one or more strong scattering peaks at various

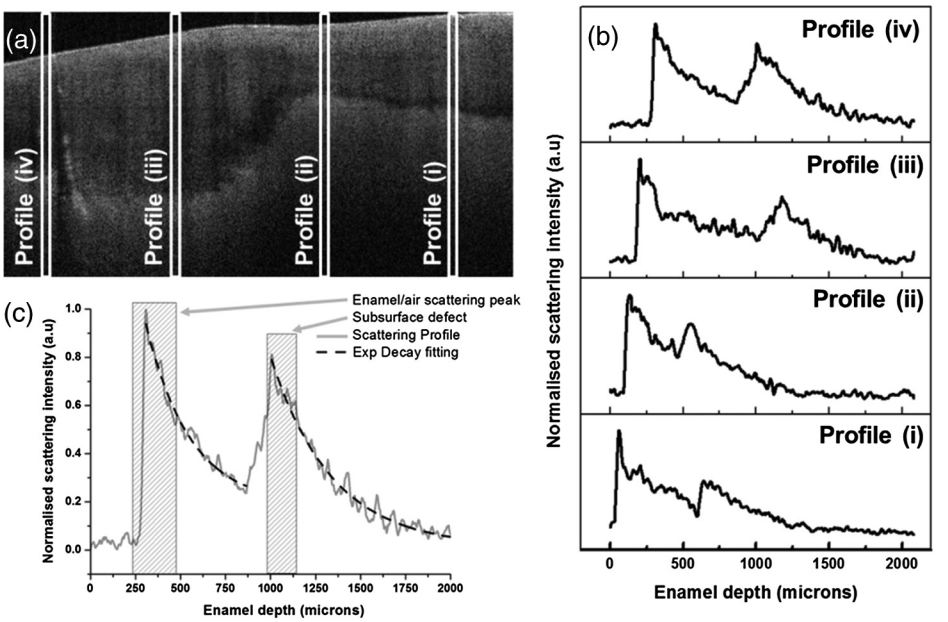

Fig. 12 (a) OCT image of MIH-affected enamel used for scattering profiles analysis selected randomly from a full stack (600 images). (b) The scattering profiles plotted at a function of enamel depth from a random location in (a) are shown. (c) A representative scattering profile observed for MIH-affected enamel is shown in greater details. This is the same tooth as in Fig. 10.

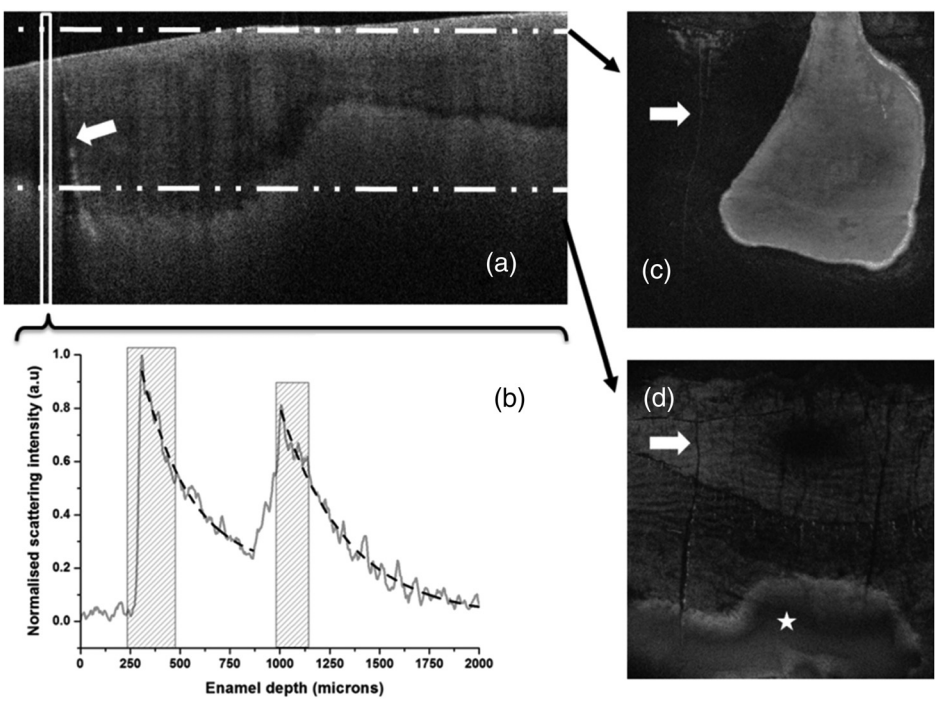

Fig. 13 Enface reconstruction of the entire OCT images stack. Frames (c) and (d) are reconstructed frames and the dot-dash-dot lines in (a) indicate the corresponding depth of both the reconstructed frames in (c) and (d). (b) The scattering profile recorded at that location in (a) and is representative of a MIH lesion. The white arrow in (a) highlights an enamel crack that is also found in (c) and (d) after the reconstruction.

distances from the enamel/air interface. The presence of these scattering peaks is indicative of a considerable local disruption of the enamel structure. From a diagnostic point of view, these scattering peaks may be used as an indicator of the depths of the enamel defect components and boundaries. For example, from the signal intensity profile in Fig. 12(b), (i) the depth to which the defect extends can be found to be 1000 μm. The ability to detect the depth below the air/enamel layer of each defect is informative, as this will inform clinicians about the depth extent of the lesion. Serial adjacent scans will inform the lateral extent of the same lesion. In Fig. 12(c), a decay that is reminiscent to that of healthy enamel can be observed between each of the two strong scattering peaks. A further approach, not presented in this paper, may be the investigation of the characteristic nature of that decay and the link with structural changes in enamel layers, healthy or not.

4.2 *Enface Reconstruction*

In order to evaluate the extent of the MIH lesions at a given depth within the tooth, the entire stack of B-scans was recomputed to create an enface reconstruction (C-scan). In this reconstruction, a frame is no longer a vertical B-scan but in fact is now a horizontal plane made of stacked rows of pixels each coming from the same Z-axis depth of the original B-scans. The full reconstruction creates a frontal section. During the reconstruction, corrective factors for the aspect ratio of individual frame are introduced so that the final dimension of each frame respects the original scanning area of 6 mm $\times$ 6 mm. Figure 13 presents an area affected by MIH discussed previously. Enface reconstruction was performed on the original dataset to evaluate the extent of the subsurface lesion. Both Figs. 13(c) and 13(d) are reconstructed frames and the dot-dash-dot lines in Fig. 13(a) indicate the corresponding depth of both the reconstructed frames in Figs. 13(c) and 13(d), respectively. Figure 13(c) shows how the surface enamel is not flat in the mesial of part of the tooth where the scan was recorded. The brighter area is indicative of the enamel, whereas the darker area is the air. As we consider the frame taken deeper within the enamel, as shown in Fig. 13(d), the lesion becomes apparent (highlighted by the star symbol). It is clearly possible to measure the extent of the lesion of interest in all three dimensions: X, Y, and Z. A significant crack is also visible in all the frames (B-scan and the two C-scans) as indicated by the arrows. This crack was used as a reference in this study to confirm the correlation between the B-scan and frames presented.

This mode of imaging represents a significant advance in both immediate diagnostics and following lesions longitudinally to ensure the management strategies chosen remain appropriate, as it enables subsurface imaging on nonprepared teeth. Provided that the full depth of the enamel can be imaged to include the EDG then, enface OCT imaging will permit its volumetric assessment. However, current data processing techniques are not yet versatile enough to allow this technology to be routinely used in a clinical setting, but it is not inconceivable to forecast that OCT (pending developments) could become a routine diagnostic tool for the assessing and treatment planning of enamel defects.

Acknowledgments

The authors would like to thank Peter Pilecki from the King's College London Dental Institute, Tissue Engineering and Biophotonics; Ministry of Higher Education and Armed Forces Medical Services, the Royal Army of Oman, Sultanate of Oman.

References

1. K. L. Weerheijm, B. Jalevik, and S. Alaluusua, "Molar-incisor hypomineralisation," *Caries Res.* **35**(5), 390–391 (2001).
2. N. S. Willmott, R. A. E. Bryan, and M. S. Duggal, "Molar-incisor-hypomineralisation: a literature review," *Eur. Arch. Paediatr. Dent.* **9**(4), 172–179 (2008).
3. S. Alaluusua, "Aetiology of molar-incisor hypomineralisation: a systematic review," *Eur. Arch. Paediatr. Dent.* **11**(2), 53–58 (2010).
4. K. L. Weerheijm et al., "Judgement criteria for molar incisor hypomineralisation (MIH) in epidemiologic studies: a summary of the European meeting on MIH held in Athens, 2003," *Eur. Arch. Paediatr. Dent.* **4**(3), 110–133 (2003).
5. F. Crombie, D. Manton, and N. Kilpatrick, "Aetiology of molar-incisor hypomineralization: a critical review," *Int. J. Paediatr. Dent.* **19**(2), 73–83 (2009).
6. D. Daly and J. M. Waldron, "Molar incisor hypomineralisation: clinical management of the young patient," *J. Ir. Dent. Assoc.* **55**(2), 83–86 (2009).
7. S. A. Fayle, "Molar incisor hypomineralisation: restorative management," *Eur. J. Paediatr. Dent.* **4**(3), 121–126 (2003).
8. K. L. Weerheijm, "Molar incisor hypomineralisation (MIH)," *Eur. J. Paediatr. Dent.* **4**(3), 114–120 (2003).
9. B. Jalevik and G. A. Klingberg, "Dental treatment, dental fear and behaviour management problems in children with severe enamel hypomineralization of their permanent first molars," *Int. J. Paediatr. Dent.* **12**(1), 24–32 (2002).
10. V. E. V. M. Beentjes, K. L. Weerheijm, and H. J. Groen, "Factors involved in the etiology of hypomineralized first permanent molars," *Ned. Tijdschr Tandheelkd.* **109**(10), 387–390 (2002).
11. FDI, Commission on Oral Health, Research and Epidemiology, "A review of the developmental defects of dental enamel index (D.D.E index)," *Int. Dent. J.* **42**(6), 411–426 (1992).
12. N. A. Lygidakis et al., "Best clinical practice guidance for clinicians dealing with children presenting with molar-incisor-hypomineralisation (MIH): an EAPD policy document," *Eur. Arch. Paediatr. Dent.* **11**(2), 75–81 (2010).
13. A. Fercher and C. Hitzenberger, "Optical coherence tomography," in *Progress in Optics*, E. Wolf, Ed., pp. 215–302, Elsevier Science B. V., Amsterdam (2002).
14. D. Huang et al., "Optical coherence tomography," *Science* **254**(5035), 1178–1181 (1991).
15. R. S. Jones et al., "Imaging artificial caries on the occlusal surfaces with polarization-sensitive optical coherence tomography," *Caries Res.* **40**(2), 81–89 (2006).
16. D. Fried et al., "Imaging caries lesions and lesion progression with polarization sensitive optical coherence tomography," *J. Biomed. Opt.* **7**(4), 618–627 (2002).
17. B. T. Amaechi et al., "Quantification of root caries using optical coherence tomography and microradiography: a correlational study," *Oral Health Prev. Dent.* **2**(4), 377–382 (2004).
18. R. S. Jones and D. Fried, "Remineralization of enamel caries can decrease optical reflectivity," *J. Dent. Res.* **85**(9), 804–808 (2006).
19. S. K. Manesh, C. L. Darling, and D. Fried, "Polarization-sensitive optical coherence tomography for the nondestructive assessment of the remineralization of dentin," *J. Biomed. Opt.* **14**(4), 044002 (2009).
20. A. M. A. Maia et al., "Characterization of enamel in primary teeth by optical coherence tomography for assessment of dental caries," *Int. J. Paediatr. Dent.* **20**(2), 158–164 (2010).
21. C. S. D. Azevedo et al., "Evaluation of caries-affected dentin with optical coherence tomography," *Braz. Oral Res.* **25**(5), 407–413 (2011).
22. R. Farah et al., "Linking the clinical presentation of molar-incisor hypomineralisation to its mineral density," *Int. J. Paediatr. Dent.* **20**(5), 353–360 (2010).
23. K. Oliver et al., "Distribution and severity of molar hypomineralisation: trial of a new severity index," *Int. J. Paediatr. Dent.* **24**(2), 131–151 (2014).

24. K. Imai et al., "Noninvasive cross-sectional visualization of enamel cracks by optical coherence tomography in vitro," *J. Endod.* **38**(9), 1269–1274 (2012).
25. T. Louie et al., "Clinical assessment of early tooth demineralization using polarization sensitive optical coherence tomography," *Lasers Surg. Med.* **42**(10), 738–745 (2010).
26. K. Hirasuna, D. Fried, and C. L. Darling, "Near-infrared imaging of developmental defects in dental enamel," *J. Biomed. Opt.* **13**(4), 044011 (2008).
27. L. L. Otis et al., "Optical coherence tomography: a new imaging technology for dentistry," *J. Am. Dent. Assoc.* **131**(4), 511 (2000).
28. I. Hariri et al., "Estimation of the enamel and dentin mineral content from the refractive index," *Caries Res.* **47**(1), 18–26 (2013).
29. Z. Meng et al., "Measurement of the refractive index of human teeth by optical coherence tomography," *J. Biomed. Opt.* **14**(3), 034010 (2009).

Khalifa Al-Azri completed his Doctorate Dentistry (Paediatrics) at the Eastman Dental Institute, University College London in 2015. The theme of his research focused on the investigation of optical coherence tomography as a clinical tool to determine the extent of molar incisor hypomineralisation lesions.

Lucia N. Melita is a conservation scientist and 4th year PhD student registered at the UCL Eastman Centre for Postgraduate Research, University College London. The theme of her research focuses on the application of nanoparticles' systems for the consolidation of organic and mineralised structures.

Adam P. Strange is a 3rd year PhD student registered at the UCL Eastman Centre for Postgraduate Research, University College London. The theme of his research focusses on the development of a nanohistology diagnostics for both connective and mineralised tissues disorders.

Frederic Festy, senior lecturer in biophotonics at King's College London Dental Institute, develops novel microscopic and spectroscopic technologies aimed at providing noninvasive optical *in-vivo* disease diagnostic tools and hard/soft tissue characterization methods.

Maisoon Al-Jawad is a senior lecturer in dental physical science in the Centre for Oral Growth and Development, Queen Mary's School of Medicine and Dentistry, Queen Mary, University of London. He research is focused on combining in-house physical techniques and central facilities such as neutron scattering and synchrotron x-ray diffraction techniques in the exploration of tooth structure and tooth/restoration complexes (crystallography); novel biomimetic hydroxyapatite surfaces (implantology); and protein adsorption events (biomineralisation/enamel formation).

Richard Cook is a senior lecturer in diagnostics and biophotonics, Hon Consultant and Clinical Lead at King's College London Dental Institute. He is dual medically and dentally qualified and has been a lead researcher for many projects over the last 15 years. He has a specific interest in developing optical diagnostics and imaging techniques for noninvasive cancer and premalignant tissue diagnosis–driven by the clinical imperative of noninvasive diagnostics and tissue surveillance, avoiding damage and adverse stimuli engendered by repeat biopsies.

Susan Parekh is a clinical lecturer and honorary consultant in pediatric dentistry at the Eastman Dental Institute, University College London. She has established a dedicated anomalies clinic, with a particular research focus on defects of enamel and dentine. She is currently the clinical lead at UCL for the development of optical coherence tomography (OCT) for the noninvasive diagnosis of enamel defects of childhood.

Laurent Bozec is a senior lecturer in biophysics and nanometrology at the Eastman Dental Institute, University College London. His research portfolio involves the nanoscale characterisation of connective and mineralised tissues to improve both fundamental knowledge in collagen and diagnostic markers of diseases such as xcleroderma, Ehlers Danlos, and centinogenesis imperfecta. Since 2012, he has also taken the challenge to expand and democratize the use of optical coherence tomography in the field of dentistry.